



SYNTHESIS OF NiCrAlX MICROPARTICLES USING DRY MILLING AND WET MILLING PROCESSES

Safitry Ramandhany^{a,b}, Djoko Triyono^{a*}, Ani Sugiarti^b, Resetiana Dwi Desiati^b, Risma Yulita Sundawa^b

^a Department of Physics, University of Indonesia
Kampus UI, Kukusan, Depok, Indonesia 16424

^b Research Center for Advanced Materials, National Research and Innovation Agency
B.J. Habibie Sains and Technology Area, Banten, Indonesia 15314

*E-mail: djoko.triyono@sci.ui.ac.id

Received: 15-05-2023, Revised: 30-06-2023, Accepted: 15-07-2023

Abstract

The characteristics of synthesized NiCrAlY and NiCrAlZr composite powders produced by the milling process were investigated to understand the particle size, the shape of particles, and the properties of crystalline structure. The milling process was carried out by combining dry milling with the wet milling method to prevent agglomeration, produce a homogeneous alloy powder, and reduce the particle size. Ethanol was used during the wet milling process as a process control agent. The PSA (particle size analysis) showed that the particle size was effectively reduced from $\pm 70 \mu\text{m}$ to less than $30 \mu\text{m}$. In addition, surface structure analysis characterized by SEM (scanning electron microscope) revealed that particle shape changed from blocky particles after dry milling into flaky, flattened, and fragmented particles after wet milling. An XRD (x-ray diffraction) was used to identify the phases of powders before and after the mechanical milling process. Crystal structure analysis was calculated from the change of peak broadening in XRD peak spectra. The Williamson-hall method has been performed to calculate the strain and crystallite size of synthesized NiCrAlY and NiCrAlZr composite powder in the present study. The findings in this study show the characteristics of powders, which are important information for producing coatings with good performance.

Keywords: Dry milling, wet milling, particle size, crystallite size, NiCrAlY, NiCrAlZr

1. INTRODUCTION

NiCrAlX (X: minor elements, i.e., Y, Zr, Hf, Ti, Si) alloys are used in TBC (thermal barrier coating) systems, which provide turbine blades with protection against oxidation and corrosion at high temperatures [1]-[3]. A critical factor against high-temperature oxidation is the performance of protective oxide on the turbine components' surface. The formation of thin, adhered, continuous, and dense protective oxide prevents the diffusion of oxidizing species [4]-[6]. In order to increase the performance of protective oxide, reactive elements such as yttrium or zirconium are added to the coating powder.

The oxidation resistance is significantly affected by porosity due to the pores acting as the diffusion paths and allowing the oxidation

species to penetrate and attack the coating and substrate [6]-[10]. One of the factors which influenced the porosity level is particle size. Reducing the particle size could reduce the level of porosity. Daroonparvar et al., investigated the effect of particle size on bond coat layer [11]. Particle size reduction using the mechanical milling and alloying method caused the formation of a continuous and dense alumina layer on the sample surface [12]-[14]. However, the dry milling method produced the agglomeration of powder. Thus, the particle size increased to $120 \mu\text{m}$ from $20 \mu\text{m}$ of the initial powder. Agglomeration conditions make the particles coarser and could be a barrier to the deposition process by blocking the nozzle gun and the high porosity level of coating.

Furthermore, Biyik and Aydin et al., studied mechanical milling parameters. The study used stearic acid in a wet milling method as a process control agent (PCA) [15]. The results obtained particle sizes of less than 35 μm , and the powder shape was flaky. PCA adsorbs the powder particles' surface and avoids the agglomeration of powder particles [16]. Ethanol was used as PCA, which could reduce the intensity of cold welding of the powder and cause flake-shaped and irregular powder formation [17].

On the other hand, characteristic of a high-energy ball mill involves deformation, fragmentation, cold welding, and structural changes such as a decrease in crystallite size and an increase in lattice strain in deformed powder. The formation of linear defects leads to a reduction in crystallite size. The crystallite size is crucial in the composite powder to evaluate its properties. The crystallite size and lattice strain are frequently calculated using integral breadth methods for line profile analysis of XRD (x-ray diffraction) peaks [18]-[19].

The simplest method used to calculate the crystallite size is Scherer's formula. However, it is applicable only when there is no strain on the materials. Other analytical methods, such as WH (Williamson hall) analysis, are generally used to determine the strain and the crystallite size of materials. It uses any peaks at lower diffraction angles to get the same information. In addition, the WH analysis is easy and suitable for strain and crystallite size calculation of cubic crystals [19]-[21].

Therefore, in this study, a combination of dry and wet milling methods was carried out to minimize the agglomeration of the powder and obtain finer particle and crystallite size. By doing these two methods, the time to reduce the size of the crystals in the powder is also shorter. The structural changes, such as crystallite size and lattice strain, were also evaluated to understand the effect of dry and wet milling combinations and the addition of the reactive element effect.

2. MATERIALS AND METHODS

2.1 Synthesis of Coating Powder

The NiCrAlY and NiCrAlZr coating powders used in the present investigation were used commercially available pure Ni, Cr, Al, Y, and Zr powder with chemical composition given in Table 1.

The mechanical milling processes were conducted in two steps: dry milling for 36 hours and wet milling for 1 hour. The wet milling was performed under ethanol to avoid the agglomeration effect. The experiment was

conducted at room temperature. A planetary ball miller (SFM-1 Desk-Top) was used to synthesize fine powders with a weight ratio of ball-to-powder of 10:1 and ball diameters of 10 mm. The revolution speeds of dry and wet milling were 1500 rpm and 1200 rpm, respectively. Some abbreviations were used in this study, such as XM, DM, and WM, which were unmilled, dry milled, and wet milled powder, respectively.

Table 1. Chemical composition of NiCrAlX powders

Coating powder	Composition (wt.%)				
	Ni	Cr	Al	Y	Zr
NiCrAlY	Bal	24	7	0.4	-
NiCrAlZr	Bal	24	7	-	0.4

2.2 Characterization

A PSA (particle size analyzer) Cilas 1190 was used to characterize the powder particle size. XRD Rigaku SmartLab (x-ray diffraction) using Cu-K α radiation that was operated at 40 kV and 30 mA for 2 θ range of 10° to 90° was used to evaluate the phase analysis of unmilled and milled powders. The FE-SEM (field emission-scanning electron microscope) JEOL JEM 2010F equipped with EDS (energy dispersive spectroscopy) Oxford X-Max 50 mm² was used to characterize the microstructure and composition of powders.

3. RESULT AND DISCUSSION

3.1 Powders Morphology

The composites of NiCrAlY and NiCrAlZr powders have been prepared by mechanical milling. Figure 1 shows the SEM (scanning electron microscope) images associated with EDS (energy dispersive spectroscopy) results of unmilled and milled powders. The unmilled powder in Figs. 1(a), and 1(d) consisted of nickel, chromium, and aluminum particles. The nickel particle was spherical; chromium and aluminum were blocky shapes. After dry milling for 36 hours, the powder SEM images, as shown in Figs. 1(b), and 1(e) showed particle powder agglomerated with irregular morphology. The agglomeration occurred because aluminum and nickel showed high ductility and flattened, resulting in cold welding [16]. According to EDS analysis, the elemental composition of the particles was uniform. It indicates that the particles mixed, forming the composite particles. Then, the wet milling method presented in Figs. 1(c), 1(f) led to flake-shaped and irregular powders forming. The flakiness of the particles after the wet milling process for 1 hour indicates that the fracturing and fragmenting stage has occurred. In addition, the presence of ethanol as

PCA could reduce the intensity of cold welding [17]. When the fragmentation rate starts to dominate over cold welding, powder refinement occurs [20]. The grain refining was led by the severe plastic deformation of particles and accumulated internal stress [19]. Based on the EDS point analysis, a homogenized distribution of elements was observed in the milled powders. The rare earth elements, i.e., yttrium and

zirconium, were not observed on the EDS analysis due to the small concentration of those elements in the composite powders. This mechanical milling process formed polycrystals on the particles.

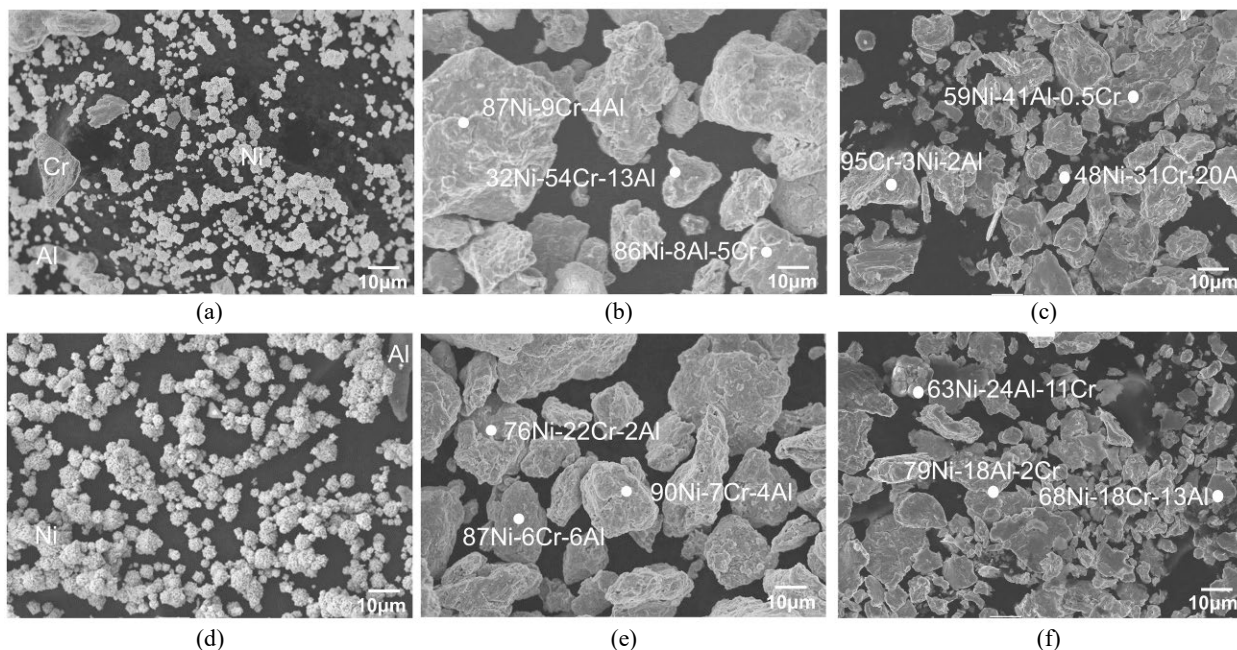


Figure 1. SEM image and EDS analysis (at%) of (a) unmilled NiCrAlY, (b) dry milled NiCrAlY, (c) dry milled followed by wet milling NiCrAlY, (d) unmilled NiCrAlZr, (e) dry milled NiCrAlZr, (f) dry milled followed by wet milling NiCrAlZr

3.2 Particle Size Distribution

Figure 2 exhibits the particle size distribution of unmilled and milled powders. The unmilled powder shows the broad particle size

distribution from the small to the bigger size. The mean size of both unmilled powders was approximately 35 μm.

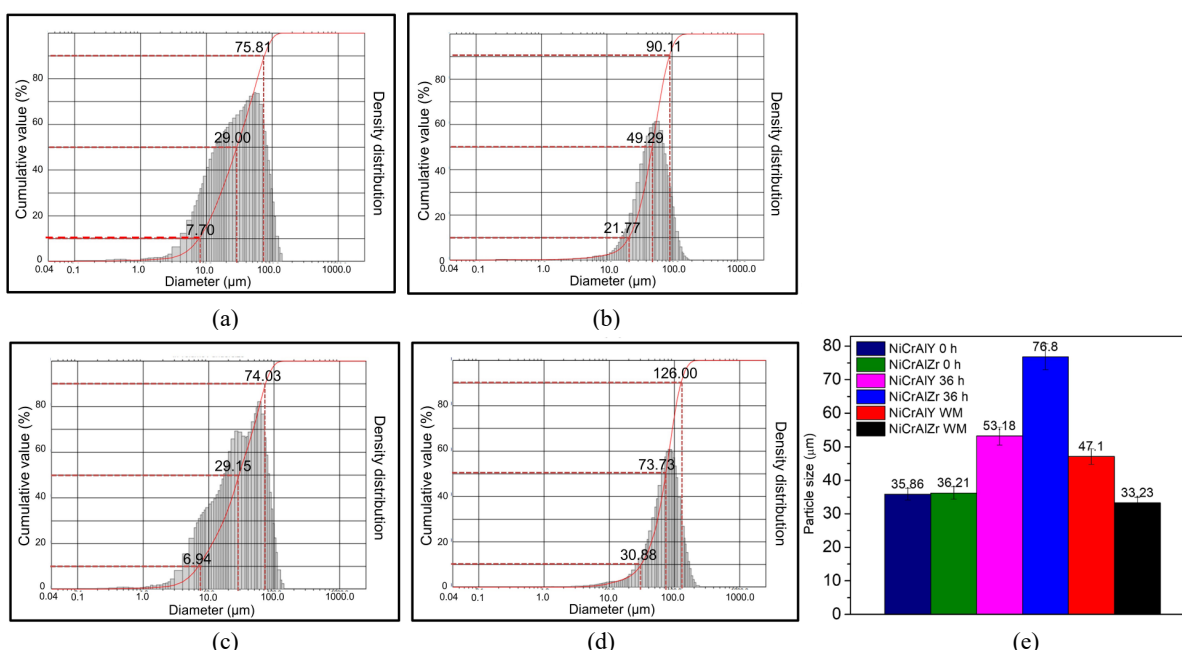


Figure 2. Particle size distribution of unmilled powder (a) NiCrAlY (c) NiCrAlZr, dry milled for 36 h of (b) NiCrAlY (d) NiCrAlZr, and average particle size of unmilled and milled powders

The dry milling process exhibited a bigger size of powders than unmilled powders. The particle distribution became narrower at the big particle size. The particle size of dry-milled powders increased up to 20-40 μm . NiCrAlZr powder showed a bigger particle size than NiCrAlY powder, approximately 53.18 μm and 76.80 μm , respectively. The fragmentation occurred after the wet milling process, resulting in a significant decrement in particle size by about 60%. It forms the flake shape particles of NiCrAlY and NiCrAlZr powders with an approximate size of 24.5 μm and 18.5 μm , respectively. SEM images presented in Fig. 1 are in correlation with the results.

3.3 Phase Identification

The XRD (x-ray diffraction) patterns of the unmilled, dry-milled, and wet-milled NiCrAlY and NiCrAlZr powders are shown in Fig. 3.

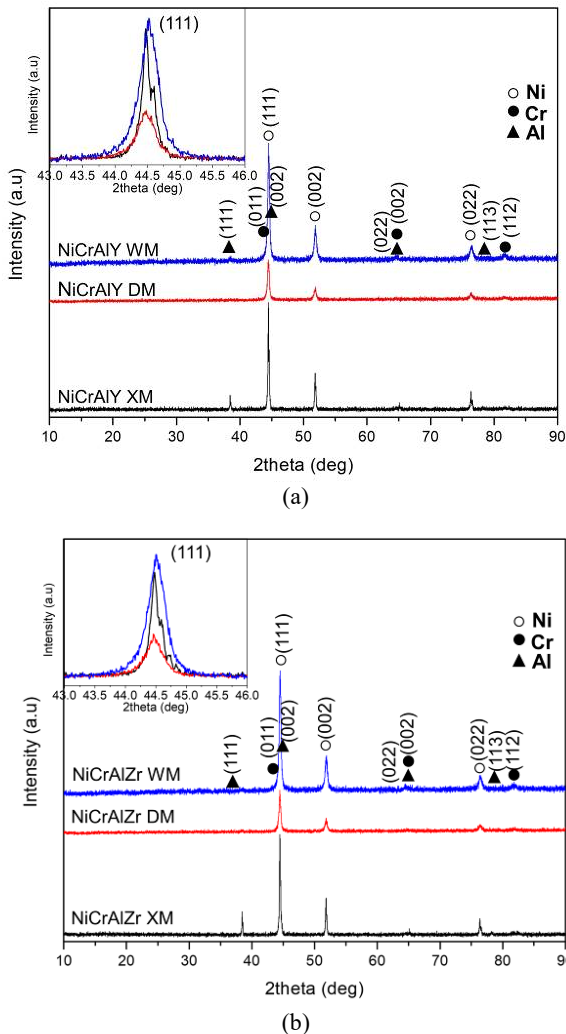


Figure 3. XRD patterns of unmilled and milled (a) NiCrAlY, (b) NiCrAlZr powders. The inset XRD pattern shows the broadening peak of the 43-46° region

The unmilled powder shows the peaks of major elements (Ni, Cr, and Al). As observed on EDS analysis, the XRD (x-ray diffraction) spectra did not detect reactive elements of yttrium and zirconium. It was due to the low composition of those reactive elements. The figure shows that the intensity of the dry-milled powder's peaks significantly decreased. Moreover, the Al peaks did not disappear on dry-milled powders. It assures that a solid solution in Ni was formed, which affects the lattice parameter of those powders [20].

In addition, the decrement in peak intensity observed on powders was due to the stress caused by mechanical milling, which generates the lattice strain. The peak intensity became high after the wet milling process, which might be due to the refinement of the crystal structure. Moreover, the diffraction line of the milled powder slightly increased the FWHM (full width at half maximum), indicating a reduction of crystallite size during mechanical milling. The inset region shows the broadening peak and the peak intensity change observed on the milled powder. The peak broadening was evaluated to calculate powders' the crystallite size and lattice strain.

3.4 X-ray Peak Broadening

To investigate the microstructural change in NiCrAlY and NiCrAlZr composite powder, the X-ray peak broadening of powders was evaluated. The broadening peaks resulting from the mechanical milling process are due to the reduction in crystallite size and the increased lattice strain caused by dislocation [22]. The diffraction peak corresponding to the instrumental corrected broadening β_{hkl} was estimated using the equation.

$$\beta_D = \{(\beta_{hkl})^2_{measured} - (\beta_{hkl})^2_{instrumental}\}^{1/2} \quad (1)$$

Scherrer's formula and Williamson-Hall's method were used to determine the crystallite size and lattice strain. These methods used the broadening of the significant element peaks, nickel peaks.

3.4.1 Williamson-Hall Analysis

The calculation of peak broadening using Scherrer's formula to measure crystallite size does not consider the strain present in the materials. However, the mechanical milling affected the XRD peak broadening due to the crystallite size and lattice strain. The crystallite size and the lattice strain contributions to peak

broadening are independent [19]. Scherrer's formula is presented in Eq. 2 [21].

$$D = \frac{k \lambda}{\beta_D \cos \theta_{hkl}} \quad (2)$$

where D is crystallite size, k is Scherrer constant (0.9), λ is the wavelength of CuK α radiation (1.5406 Å), β_{hkl} is the full width at half maximum (FWHM) in radians, θ_{hkl} is Bragg's angle of diffraction lines.

3.4.1.1 Uniform Deformation Model

Strain-induced broadening arising from defects like imperfections and distortions are related by Eq. (3).

$$\varepsilon \sim \frac{\beta_D}{\tan \theta_{hkl}} \quad (3)$$

The WH analysis is suitable for calculating the crystallite size and lattice strain. Since the crystallite size and lattice strain could independently affect the peak broadening, the strain-induced peak broadening β_s is given by the relation:

$$\beta_s = 4 \varepsilon \tan \theta \quad (4)$$

$$\beta_{hkl} = \beta_D + \beta_s \quad (5)$$

$$\beta_{hkl} = \frac{k \lambda}{D \cos \theta_{hkl}} + 4 \varepsilon \tan \theta \quad (6)$$

$$\beta_{hkl} \cos \theta = \frac{k \lambda}{D} + 4 \varepsilon \sin \theta \quad (7)$$

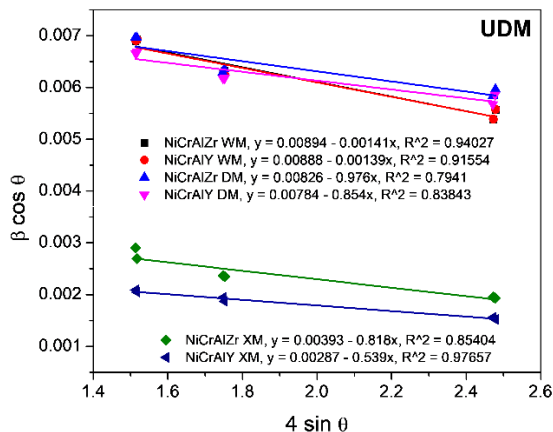


Figure 4. The Williamson-Hall analysis of unmilled and milled NiCrAlY and NiCrAlZr powder using UDM assumption

Eq. (7) represents the UDM (uniform deformation model). The plot is drawn between $\beta \cos \theta$ and $4 \sin \theta$. The crystallite size and lattice strain are derived from the intercept ($c = k\lambda/t$) and the slope ($m = \varepsilon$), respectively. The UDM equation assumed that strain was uniform in all crystallographical directions. In addition, this calculation considers the isotropic nature of the crystal, which the properties of materials do not depend on the direction. The W-H analysis using

the UDM assumption is presented in Fig. 4. Meanwhile, the calculation of crystallite size and lattice strain using the UDM assumption is shown in Table 2.

3.4.1.2 Uniform Stress Deformation Model

UDM considers uniform strain present in all crystallographic directions. The strain of mechanical milling powders, on the other hand, is not uniform in all directions. USD (uniform stress deformation model) generalized Hooke's law refers to the lattice strain. The strain and stress are in linear proportionality.

$$\sigma = E_{hkl} \varepsilon \quad (8)$$

where σ is the stress, E_{hkl} is the modulus of elasticity, and ε is the strain.

The modulus of elasticity of the cubic FCC (faced center cubic) crystal along the direction of (h k l) is

$$\frac{1}{E_{hkl}} = S_{11} - 2(S_{11} - S_{12} - 0.5S_{44})(h^2 k^2 + k^2 l^2 + l^2 h^2)/(h^2 + k^2 + l^2)^2 \quad (9)$$

where S_{11} , S_{12} , and S_{44} are the elastic compliances of pure Ni with values of 7.34×10^{-3} , 2.74×10^{-3} , and $8.02 \times 10^{-3} \text{ GPa}^{-1}$, respectively. The y-intercept of $\beta_{hkl} \cos \theta_{hkl}$ versus $4 \sin \theta_{hkl}/E_{hkl}$ graph, the uniform stress (σ) and the lattice strain (ε), which are derived from the slope of the mentioned graph, can be used to determine the crystallite size (D). The USD model for unmilled and milled powder calculation is exhibited in Fig. 5. The value of crystallite size, stress, and the lattice strain estimated by USD is presented in Table 2. A minor strain can be validly estimated using this equation.

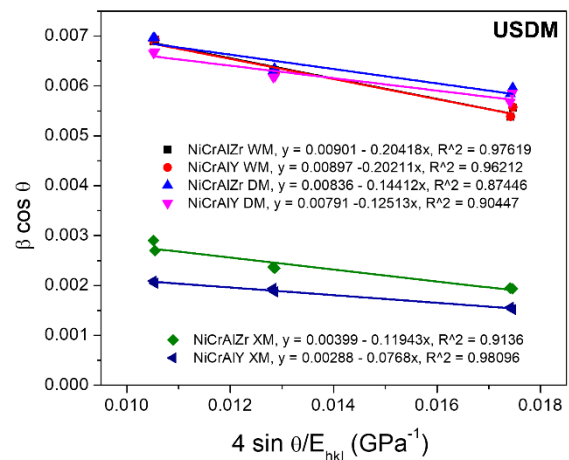


Figure 5. The Williamson-Hall analysis of unmilled and milled NiCrAlY and NiCrAlZr powder assuming USD

3.4.1.3 Uniform Deformation Energy-Density Model

In USDM, it considers a linear proportionality between stress and strain. However, it no longer remains linear when the strain energy density (u) is considered. In the UDEDM (uniform deformation energy-density model), the cause of anisotropic strain is assumed to be deformation energy density (energy per unit). The energy density for an elastic system following Hooke's law can be determined from $u = (\epsilon^2 E_{hkl})/2$. Then according to the energy and strain relation, the equation can be modified as presented in Eq. 10.

$$\beta_{hkl} \cos \theta = \left(\frac{k\lambda}{D}\right) + \left(4 \sin \theta \left(\frac{2u}{E_{hkl}}\right)^{1/2}\right) \quad (10)$$

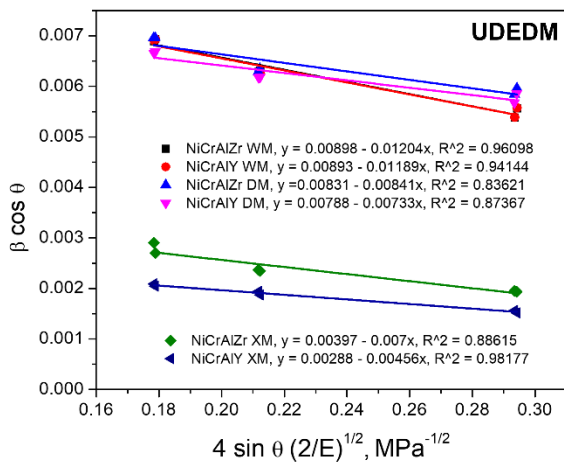


Figure 6. The Williamson-Hall analysis of unmilled and milled NiCrAlY and NiCrAlZr powder assuming UDEDM

The UDEDM graph was constructed of $\beta_{hkl} \cos \theta$ versus $4 \sin \theta \left(\frac{2u}{E_{hkl}}\right)^{1/2}$. The intercept used to determine the crystallite size (D) was

calculated from the intercept, the slope of the line used to determine the anisotropic energy density and the lattice strain. The crystallite size and energy density are exhibited in Table 2.

According to the previous studies, in which crystallite size was determined using the Williamson-Hall method and then compared with the TEM (transmission electron microscope) image, the UDEDM anisotropy model could be a suggested realistic model, especially for milled powders.

Williamson-Hall's model of unmilled and milled NiCrAlY and NiCrAlZr showed a negative slope, indicating a negative strain, which might be due to the lattice shrinkage [23]. The crystallite size of milled powders calculated using UDM, USDM, and UDEDM shows the decrement. The crystallite size decrement of dry milled powder is up to 64%, from approximately 50 nm to 18 nm. Meanwhile, the difference in crystallite size of dry-milled and wet-milled powder was about 1 nm, and wet milled powder showed a smaller crystallite size. The formation of linear defects induces the reduction of crystallite size [19].

In contrast, increasing the milling time causes an increase in lattice strain. The crystal imperfection, such as point defect and dislocation, affects the lattice strain. It was due to the high-energy collision between the ball mill and vial in the mechanical milling process [24]. The stress and deformation energy also increases with the increase of milling time.

Table 2. Crystallite size and lattice strain of NiCrAlY and NiCrAlZr powders

Sample condition	Williamson-Hall method							
	UDM		USDM			UDEDM		
	D, nm	ϵ ($\times 10^{-3}$)	D, nm	σ (10^{-1} GPa)	ϵ ($\times 10^{-3}$)	D, nm	u, kJ/m ³	ϵ ($\times 10^{-3}$)
NiCrAlY XM	50.46 \pm 0.99	0.54 \pm 0.04	50.28 \pm 2.18	0.768 \pm 0.048	0.53 \pm 0.03	50.28 \pm 2.24	0.021 \pm 0.007	0.54 \pm 0.01
NiCrAlZr XM	36.85 \pm 0.50	0.82 \pm 0.15	37.13 \pm 8.64	1.190 \pm 0.163	0.83 \pm 0.11	36.48 \pm 0.56	0.049 \pm 0.001	0.83 \pm 0.13
NiCrAlY DM	18.47 \pm 0.45	0.87 \pm 0.16	18.31 \pm 0.58	1.251 \pm 0.180	0.87 \pm 0.13	18.57 \pm 0.51	0.049 \pm 0.002	0.83 \pm 0.15
NiCrAlZr DM	17.53 \pm 0.34	0.97 \pm 0.17	17.32 \pm 0.43	1.441 \pm 0.241	1.00 \pm 0.07	17.48 \pm 0.38	0.071 \pm 0.003	0.99 \pm 0.19
NiCrAlY WM	16.31 \pm 0.39	1.39 \pm 0.19	16.14 \pm 0.58	2.021 \pm 0.179	1.40 \pm 0.12	17.88 \pm 0.47	0.141 \pm 0.002	1.40 \pm 0.16
NiCrAlZr WM	16.20 \pm 0.47	1.41 \pm 0.16	16.07 \pm 0.73	2.042 \pm 0.142	1.42 \pm 0.10	16.13 \pm 0.57	0.145 \pm 0.001	1.41 \pm 0.03

4. CONCLUSION

NiCrAlY and NiCrAlZr powders have been synthesized using a mechanical milling process resulting in a homogenous powder and were characterized by XRD (x-ray diffraction), PSA (particle size analysis), and SEM (scanning electron microscope). The mechanical milling process was divided into two stages: dry and wet. The dry milling process produced the agglomerated NiCrAlX powders. The particle size value of the is approximately 70 μm due to the high ductility of the element. The wet milling process using ethanol as a process control agent could reduce the particle size significantly up to $\pm 30 \mu\text{m}$.

After dry milling for 36 hours, followed by wet milling for 1 hour, the phase change of the powder did not occur. However, the disappearance of the Al peak was observed in dry-milled powder, assuming due to the solid solution formation. The dominant element of Ni shows the FCC (face centered cubic) structure. The evaluation of the dominant element broadening peak was done by W-H analysis. XRD patterns of milled powder exhibited the line broadening due to the reduction in crystallite size and increased lattice strain. The values of crystallite size and lattice strain of milled NiCrAlY and NiCrAlZr were approximately 16 nm and 1.4×10^{-3} , respectively. The influence of reactive element addition on the powder's crystallite size and lattice strain is not observed. In conclusion, the mechanical milling process produces good powder coating characteristics, leading to good coating performance.

ACKNOWLEDGMENT

The authors would like to thank the research project from the National Research and Innovation Agency (BRIN) with contract No. 3/III.10/HK/2023 for supporting the present research work.

REFERENCES

- [1] F. Ghadami, A. S. R. Aghdam, and S. Ghadami, "Microstructural characteristics and oxidation behavior of the modified MCrAlX coatings: A critical review," *Vacuum*, vol. 185, 2021. Doi: 10.1016/j.vacuum.2020.109980.
- [2] Y. Huang, Y. He, B. Yang, A. Khan, X. Zhao, and P. Song, "Effect of YSZ/TaSi₂-MCrAlY thermal barrier coatings on oxidation resistance in air and water vapor," *Ceram. Int.*, vol. 49, pp. 14551-14562, 2023. Doi: 10.1016/j.ceramint.2023.01.045.
- [3] J. G. Thakare, C. Pandey, M. M. Mahapatra, and R. S. Mulik, "Thermal barrier coatings-A state of the art review," *Met. Mater. Int.*, vol. 27, no. 7, pp. 1947-1968, 2021. Doi: 10.1007/s12540-020-00705-w.
- [4] K. M. Doleker, Y. Ozgurluk, and A. C. Karaoglanli, "TGO growth and kinetic study of single and double layered TBC systems," *Surf. Coatings Technol.*, vol. 415, 2021. Doi: 10.1016/j.surfcoat.2021.127135.
- [5] A. Sezavar, S. A. Sajjadi, A. Babakhani, R. L. Peng, and K. Yuan, "Oxidation behavior of a nanostructured compositionally graded layer (CGL) thermal barrier coating (TBC) deposited on IN-738LC," *Surf. Coatings Technol.*, vol. 374, no. March, pp. 374-382, 2019. Doi: 10.1016/j.surfcoat.2019.06.024.
- [6] B. J. Harder, "Oxidation performance of Si-HFO₂ environmental barrier coating bond coats deposited via plasma spray-physical vapor deposition," *Surf. Coatings Technol.*, vol. 384, pp. 2-9, 2020. Doi: 10.1016/j.surfcoat.2019.125311.
- [7] S. K. Essa, K. Chen, R. Liu, X. Wu, and M. X. Yao, "Failure mechanisms of APS-YSZ-CoNiCrAlY thermal barrier coating under isothermal oxidation and solid particle erosion," *J. Therm. Spray Technol.*, vol. 30, no. 1-2, pp. 424-441, 2021. Doi: 10.1007/s11666-020-01124-4.
- [8] J. Shi, T. Zhang, B. Sun, B. Wang, X. Zhang, and L. Song, "Isothermal oxidation and TGO growth behavior of NiCoCrAlY-YSZ thermal barrier coatings on a Ni-based superalloy," *J. Alloys Compd.*, vol. 844, p. 156093, 2020. Doi: 10.1016/j.jallcom.2020.156093.
- [9] D. H. Kim, K. K. Kim, B. W. Moon, K. B. Park, S. Park, and C. S. Seok, "Prediction of growth behavior of thermally grown oxide considering the microstructure characteristics of the top coating," *Ceram. Int.*, vol. 47, no. 10, pp. 14160-14167, 2021. Doi: 10.1016/j.ceramint.2021.02.003.
- [10] G. An, W. Li, L. Feng, B. Cheng, Z. Wang, Z. Li, and Y. Zhang, "Isothermal oxidation and TGO growth behaviors of YAG/YSZ double-ceramic-layer thermal barrier coatings," *Ceram. Int.*, vol. 47, no. 17, pp. 24320-24330, 2021. Doi: 10.1016/j.ceramint.2021.05.144.
- [11] M. S. Hussain and M. Daroonparvar, "The

- synthesis of nanostructured NiCrAlY powders for plasma sprayed thermal barrier coatings,” *Adv. Phys. Theor. dan Appl.*, vol. 13, pp. 1-9, 2013.
- [12] J. Lu, Y. Chen, H. Zhang, C. Zhao, X. Zho, F. Guo, and P. Xiao, “Superior oxidation and spallation resistant NiCoCrAlY bond coat via homogenizing the yttrium distribution,” *Corros. Sci.*, vol. 159, pp. 2019. Doi: 10.1016/j.corsci.2019.108145.
- [13] H. Vasudev, L. Thakur, A. Bansal, H. Singh, and S. Zafar, “High temperature oxidation and erosion behaviour of HVOF sprayed bi-layer Alloy-718/NiCrAlY coating,” *Surf. Coatings Technol.*, vol. 362, pp. 366-380, 2019. Doi: 10.1016/j.surcoat.2019.02.012.
- [14] A. Zakeri, E. Bahmani, A. S. R. Aghdam, B. Saeedi, and M. Bai, “A study on the effect of nano-CeO₂ dispersion on the characteristics of thermally-grown oxide (TGO) formed on NiCoCrAlY powders and coatings during isothermal oxidation,” *J. Alloys Compd.*, vol. 835, p. 155319, 2020. Doi: 10.1016/j.jallcom.2020.155319.
- [15] S. Biyik and M. Aydin, “Characterization of nanocrystalline Cu₂₅Mo electrical contact material synthesized via ball milling,” *Acta Phys. Pol. A*, vol. 132, no. 3, pp. 886-888, 2017. Doi: 10.12693/APhysPolA.132.886.
- [16] C. Suryanarayana, “Mechanical alloying: a novel technique to synthesize advanced materials,” *Research*, vol. 2019, p. 4219812, 2019. Doi: 10.34133/2019/4219812.
- [17] A. Zakeri, F. Ghadami, A. S. Rouhaghdam, and B. Saeedi, “Study on production of modified MCrAlY powder with nano oxide dispersoids as HVOF thermal spray feedstock using mechanical milling,” *Mater. Res. Express*, vol. 7, no. 1, p. 015030, 2019. Doi: 10.1088/2053-1591/ab6121.
- [18] A. A. Eze, E. R. Sadiku, W. K. Kupolati, J. Syman, J. M. Ndambuki, T. Jamiru, M. O. Durowoju, I. D. Ibrahim, M. B. Shongwe, and D. A. Desai, “Wet ball milling of niobium by using ethanol, determination of the crystallite size and microstructures,” *Sci. Rep.*, vol. 11, no. 1, pp. 1-8, 2021. Doi: 10.1038/s41598-021-01916-w.
- [19] S. Sivasankaran, K. Sivaprasad, R. Narayanasamy, and P. V. Satyanarayana, “X-ray peak broadening analysis of AA 6061100-x-x wt.% Al₂O₃ nanocomposite prepared by mechanical alloying,” *Mater. Charact.*, vol. 62, no. 7, pp. 661-672, 2011. Doi: 10.1016/j.matchar.2011.04.017.
- [20] D. Singh and R. Kumar, “Synthesis and characterization of nanocrystalline Ni-Cr-Al alloy powder,” *Mater. Today Proc.*, vol. 41, pp. 821-824, 2020. Doi: 10.1016/j.matpr.2020.09.155.
- [21] P. S. Sundaram, T. Sangeetha, S. Rajakarthishan, R. Vijayalaksmi, and A. Elangovan, “XRD structural studies on cobalt doped zinc oxide nanoparticles synthesized by coprecipitation method: Williamson-Hall and size-strain plot approaches,” *Phys. B Phys. Condens. Matter*, vol. 595, p. 412342, 2020. Doi: 10.1016/j.physb.2020.412342.
- [22] R. Kumar, S. R. Bakshi, J. Joardar, S. Parida, V. S. Raja, and R. K. Singh Raman, “Structural evolution during milling, annealing, and rapid consolidation of nanocrystalline Fe-10Cr-3Al powder,” *Materials (Basel)*, vol. 10, no. 3, pp. 25-27, 2017. Doi: 10.3390/ma10030272.
- [23] A. K. Zak, W. H. Abd. Majid, M. E. Abrishami, and R. Yousefi, “X-ray analysis of ZnO nanoparticles by Williamson-Hall and size-strain plot methods,” *Solid State Sci.*, vol. 13, no. 1, pp. 251-256, 2011. Doi: 10.1016/j.solidstatesciences.2010.11.024.
- [24] H. Irfan, K. M. Racik, and S. Anand, “Microstructural evaluation of CoAl₂O₄ nanoparticles by Williamson-Hall and size-strain plot methods,” *J. Asian Ceram. Soc.*, vol. 6, no. 1, pp. 54-62, 2018. Doi: 10.1080/21870764.2018.1439606.